

# Analyzing Multispectral Satellite Imagery of South American Wildfires Using Deep Learning

Christopher Sun

March 2022

## Abstract

Since severe droughts are occurring more frequently and lengthening the dry season in the Amazon Rainforest, it is important to detect wildfires promptly and forecast possible spread for effective suppression response. Though computer vision researchers have applied algorithms to automatically detect wildfires, current models are computationally expensive and not versatile enough for the low technology conditions of South American wildfire hotspots. This comprehensive deep learning study first trains a Fully Convolutional Neural Network with skip connections on multispectral Landsat 8 images of Ecuador and the Galapagos. The model uses Green and Short-wave Infrared (SWIR) bands as inputs to predict each image's corresponding pixel-level binary fire mask. This model achieves a 0.962 validation F2 score and a 0.932 F2 score on test data from Guyana and Suriname. Afterward, image segmentation is conducted on the Cirrus band using K-Means Clustering to simplify continuous pixel values into three discrete classes representing differing degrees of cirrus cloud contamination. Two additional Convolutional Neural Networks are trained to classify the presence of a wildfire using these segmented cirrus images. The "experimental" model trained on the segmented inputs and SWIR data achieves a binary accuracy that is 2.306% higher than that of the "benchmark model" that is trained only on SWIR data. The difference in performance has a p-value of 0.00968. This proof of concept reveals that feature simplification can improve the performance of wildfire detection models. Overall, the software built in this study is useful for early and accurate detection of wildfires in South America.

# Contents

<b>1</b>	<b>Introduction</b>	<b>3</b>
1.1	Research Outline . . . . .	3
<b>2</b>	<b>Materials and Data</b>	<b>3</b>
2.1	Landsat 8 Imagery . . . . .	3
<b>3</b>	<b>Methods</b>	<b>4</b>
3.1	Preprocessing . . . . .	4
3.2	Fully Convolutional Neural Network . . . . .	5
3.2.1	Neural Network Design . . . . .	5
3.2.2	Loss and Metric Functions . . . . .	6
3.2.3	Training . . . . .	6
3.3	Cirrus Band Analysis . . . . .	7
3.3.1	Cirrus Data Preparation . . . . .	7
3.3.2	K-Means Clustering for Unsupervised Cirrus Image Segmentation . . . . .	7
3.3.3	Cirrus-to-Wildfire CNN . . . . .	7
<b>4</b>	<b>Results</b>	<b>8</b>
4.1	Fully Convolutional Neural Network . . . . .	8
4.1.1	Learning Curves . . . . .	8
4.1.2	Metrics and Confusion Matrix . . . . .	9
4.1.3	Performance Visualizations . . . . .	9
4.1.4	Model Testing Scenarios . . . . .	12
4.2	Cirrus Band Analysis . . . . .	12
4.2.1	Unsupervised Image Segmentation . . . . .	12
4.2.2	Learning Curves and Metrics . . . . .	13
4.2.3	Two Proportion Z-Test . . . . .	13
<b>5</b>	<b>Discussion</b>	<b>14</b>
5.1	Deep Learning Tasks . . . . .	14
5.1.1	FCN . . . . .	14
5.1.2	Cirrus-to-Wildfire CNN . . . . .	14
5.2	Relationship Between Cirrus Clouds and Wildfire Acreage . . . . .	15
<b>6</b>	<b>Conclusions</b>	<b>15</b>

# 1 Introduction

In places like the Amazon Rainforest, where severe droughts are occurring more frequently and lengthening the dry season, interconnected ecosystems are threatened by more widespread occurrences of wildfires (Aragão et al. 2018) [1]. It is not only important to respond to wildfires promptly using well-informed allocation of rescue resources to minimize waste, but also to forecast active wildfires before they become inextinguishable. Progress towards this task has been made in the field of computer vision, with researchers applying machine learning algorithms on large databases to automatically detect wildfires. Matson and Holben (1987) used remote sensing techniques like Dozier’s method to extract pixel-level information from NOAA data of regions in Brazil [8]. More recently, Schroeder et al. (2016) used the Near-Infrared and Short-Wave Infrared bands from the Landsat 8 satellite to classify fire-affected pixels. The researchers achieved a very low rate of false positives [13]. Khryashchev and Larionov (2020) used RGB images and data augmentation for wildfire detection [5]. Similarly, Sousa et al. (2020) employed transfer learning on an augmented data set of fire events in Portugal [14]. Pereira et al. (2021) introduced three deep convolutional neural network architectures for active wildfire detection, using these models to predict the overhead pixel-level labels of a 256 x 256 pixel patch of land [11].

## 1.1 Research Outline

The following sections of this work detail a comprehensive deep learning study conducted on multispectral geospatial data of Ecuador and the Galapagos from the Landsat 8 satellite [7]. After preprocessing of the data, a fully convolutional neural network (FCN) with skip connections is trained on 3-channel image inputs to predict the corresponding fire mask. The paper then takes a deeper dive into one specific spectral band, the Cirrus Cloud band, describing an unsupervised learning approach to image segmentation. After the pixels of each cirrus image are segmented into discrete classes of cirrus contamination, two more convolutional neural networks are trained to investigate the effect of feature simplification on model performance. The results reveal that feature simplification can not only improve model performance but also be useful when computational resources are scarce. Finally, data analysis on cirrus cloud imagery hints at an underlying correlation between cirrus contamination and occurrences of wildfires.

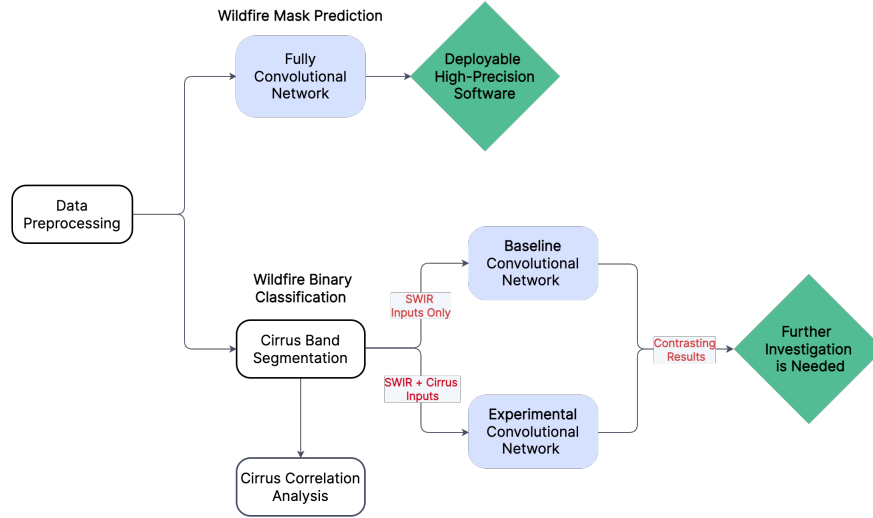


Figure 1: Experimental Design

## 2 Materials and Data

### 2.1 Landsat 8 Imagery

The data used for this research was a subset of a large publicly available database of Landsat 8 satellite images [10] processed by Pereira et al. (2021) [11]. Of the entire South American continent, aerial images of Ecuador and the

Galapagos were selected to train the model, and images of Guyana and Suriname were used as test data for a final model evaluation. The Landsat 8 satellite uses a Worldwide Reference System (WRS) denoted by path-row pairs. Each path-row pair covers approximately a 115 x 112 mile area (Knight and Knight 2014), with some overlap between pairs [7]. The regions of Ecuador and the Galapagos from which the data for this research was acquired is shown below, divided according to the WRS.

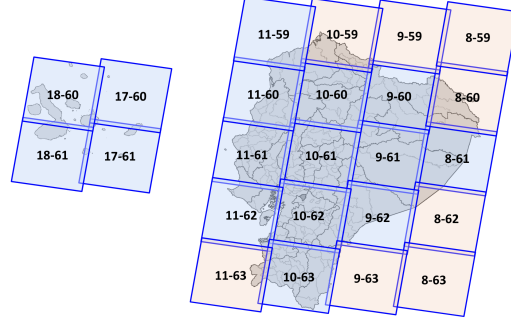


**Figure 2:** Landsat WRS. The data used for the models in this research was acquired from areas shaded in blue.

The data consisted of 14,823 images containing at least one region with an active fire, and 11,848 containing no fires in any pixels. The former set of images will be referred to as the “fire” images and the latter as the “non-fire” images. Each georeferenced TIFF had dimensions of 128 x 128 pixels x 10 spectral bands.<sup>1</sup> Each image was paired with its corresponding pixel-level label called a mask. The masks were composed of 0s and 1s, where a “0” pixel value indicates the absence of fire and a “1” pixel value indicates the presence of fire in that region. These 128 x 128 pixel masks were either manually annotated or generated according to the conditions described in Schroeder et al. (2016) [13].

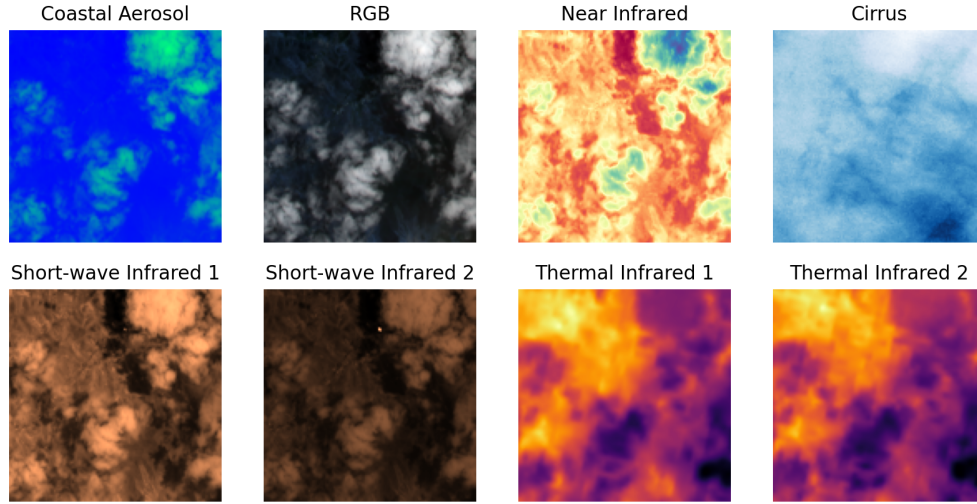


**Figure 3:** An example of one 10-band image in the data set. The three RGB bands are visualized as one band.

### 3 Methods

#### 3.1 Preprocessing

Some 10-band images had a large number of pixels that were 0, the reasons for which were unknown.<sup>2</sup> After elimination of these images, the data set was narrowed down to 14,274 “fire” images. “Non-fire” images were not included as

<sup>1</sup>Though Landsat 8 Operational Land Imager (OLI) and Thermal Infrared Sensor (TIRS) images have 11 bands, the Panchromatic band with 15 meters resolution was excluded at the discretion of the researchers who processed the data.

<sup>2</sup>This might have been due to the fact that they were acquired at the *borders* of WRS path-row grids.

data for the wildfire detection model, for reasons described in Section 3.2.3.

**Class Imbalance** The data set contained extreme class imbalance, as the masks of the “fire” images consisted of overwhelmingly more “non-fire” pixels than “fire” pixels. The median number of fire pixels in each mask was 2 pixels<sup>3</sup>. Using Landsat 8’s resolution of 30 meter per pixel, this equates to a 3,840 x 3,840 squared meter (3644 acre) patch of land only having 1900 square meters (0.445 acres) of active wildfire, on average.

## 3.2 Fully Convolutional Neural Network

### 3.2.1 Neural Network Design

Given the images and masks in the data set, the ultimate modeling task was to extract features from each image to predict the corresponding mask. Accomplishing this task would not require all ten bands of data, as demonstrated by Pereira et al. (2021), who used only three bands and generated good results [11]. Consequently, the Landsat-8 bands selected as inputs to predict the wildfire masks were the Green and Short-wave Infrared bands. The deep learning model assembled for this task was based off of the U-Net, a deep Fully Convolutional Network (FCN) used for biomedical image segmentation tasks (Ronneberger et al. 2015) [12]. Instead of the four downsampling and upsampling blocks in the U-Net, this model was a shallower model consisting of only three blocks, with less filters as well. As a result, the model had only 2,138,785 trainable parameters.

During the downsampling phase, 2D convolution layers enlarge the number of channels, while maximum pooling reduces dimensionality along the first and second axes of the input. While the input shape is 128 x 128 x 3, the bottleneck layer has dimensions of 16 x 16 x 128. During the upsampling phase, transposed convolution (deconvolution) layers reduce the number of channels and increase dimensionality along the first and second axes. In essence, the image is encoded by the model, and after passing through a bottleneck phase, is decoded back towards the shape of the input image. Skip connections between the first and seventh, second and sixth, and third and fifth blocks bypass interior layers of the model, providing feature information to later layers that might be lost from downsampling (Drozdzal et al. 2016) [4]. A final 1 x 1 convolution layer generates the 128 x 128 x 1 output mask.

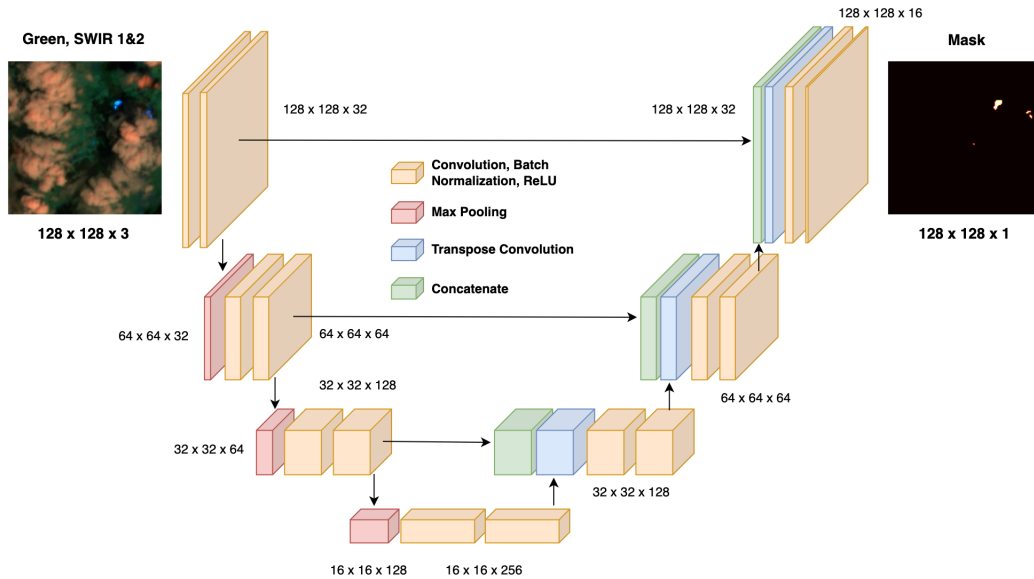


**Figure 4:** The U-Net-inspired Fully Convolutional Model built for the mask prediction task.

<sup>3</sup>Each mask contained 16,384 pixels

### 3.2.2 Loss and Metric Functions

Due to the class imbalance in the image masks, the model required a weighted loss function. The standard binary cross-entropy loss function used for binary classification was adjusted by a factor of  $\mathbf{p_c}$ , called the class weight. This class weight was computed using:

$$\mathbf{p_c} = \frac{\text{Total number of pixels that equal 0}}{\text{Total number of pixels that equal 1}} = \frac{\text{Total number of pixels in dataset}}{\text{Total number of pixels that equal 1}} - 1.$$

Accordingly, the loss function was defined as:

$$L(\theta) = \frac{1}{m} \cdot \sum_{i=1}^m \sum_{n=1}^k \left[ \mathbf{p_c} \cdot y^{(n)} \cdot \log(h(x^{(n)})) + (1 - y^{(n)}) \cdot \log(1 - h(x^{(n)})) \right]^i,$$

where  $k$  is the number of pixels in each flattened mask,  $y^{(n)}$  is the ground truth classification of the  $n^{th}$  pixel,  $h(x^{(n)})$  is the prediction value of the  $n^{th}$  pixel, and a summation is applied over every pixel of the  $i^{th}$  image for a total of  $m$  images in each mini-batch.

The F-beta score with a beta value of 2 was used as a performance metric for the FCN.<sup>4</sup> Let precision  $P = \frac{tp}{tp+fp}$  and let recall  $R = \frac{tp}{tp+fn}$ , where  $tp$  (true positives) is the number of pixels containing wildfires that are correctly classified by the model,  $fp$  (false positives) is the number of pixels without wildfires but classified otherwise by the model, and  $fn$  (false negatives) is the number of pixels containing wildfires but classified otherwise by the model. The F-beta score is then:

$$F_\beta = \frac{1 + \beta^2}{\frac{\beta^2}{P} + \frac{1}{R}} = \frac{(1 + \beta^2)PR}{\beta^2 P + R}.$$

The  $F_2$  is a weighted harmonic mean of the precision and recall, with more weight given to the recall. Theoretically, maximizing the recall should be prioritized over maximizing the precision, since in scenarios where wildfire prediction software will be used, it is more important to minimize false negatives than false positives (Arana-Pulido et al. 2018) [2]. When a region is mistakenly assessed as wildfire-free, fire-extinguishing resources will not be allocated to that region, meaning the fire could expand while rescuers are not aware. Hence, the  $F_2$  score, given below, was selected as a performance metric for the FCN.<sup>5</sup>

$$F_2 = \frac{5PR}{4P + R}.$$

Substituting  $P$  and  $R$  in terms of their components,

$$F_2 = \frac{tp}{tp + 0.2fp + 0.8fn}.$$

### 3.2.3 Training

The FCN was optimized using Adam optimization (Kingma and Ba 2014) [6] with an exponentially decaying learning rate. The learning rate  $\alpha$  as a function of the epoch of training,  $t$ , was

$$\alpha(t) = \alpha_0 e^{-0.1t},$$

where  $\alpha_0$  was 1e-3 and 0.1 was a hyperparameter. The ReLU activation function was used throughout the model, with the exception of the last layer which used the sigmoid function. Batch Normalization on the channels axis had a regularizing effect on the model (Dauphin and Cubuk 2020) [3], as no other regularization techniques had to be applied. The model was trained for 100 epochs with a mini-batch size of 32 images.

Only the 14,247 “fire” images were used as data for training the neural network; the 11,848 “non-fire” images were excluded. As explained in Section 3.1, very few pixels on average contained fires. Hence, in order for the model to

<sup>4</sup>Binary accuracy was not a reasonable metric since image masks contained overwhelmingly more 0s than 1s. If the model learned nothing and predicted a mask of pure 0s for every images, its binary accuracy would be extremely high, but this would be a misinformed metric.

<sup>5</sup>As the  $F_1$  score is more widely used, the  $F_1$  score will also be provided in Section 4.1.2 to allow for comparison with other published models.

achieve a high  $F_2$  score, it must be a very good discriminator between the classification of each pixel. It follows that if the model can already discern exactly which few pixels (out of 16,384) have fires, there is little additional benefit from adding more data images that have masks of purely 0's. A 85-15% train-validation split created a train set with 12,132 images and a validation set with 2,142 images.

### 3.3 Cirrus Band Analysis

Environmental research has shown that there are subtleties in atmospheric responses to wildfires that provide information about the sources of the fires themselves. One such example, as highlighted by Veselovskii et al. (2021) [17], is the association of wildfire smoke with cirrus clouds. The authors found that smoke properties such as surface area, volume, and concentration could be extracted simultaneously with cirrus properties, using multispectral LiDAR observations.

The ideas of the authors motivated another avenue of experimentation: extracting features from the cirrus bands for the binary classification of the presence of a wildfire, as a proof of concept for feature simplification.

#### 3.3.1 Cirrus Data Preparation

Before training a neural network, the cirrus bands needed to be preprocessed. Since not all images in the data set contained cirrus cloud contamination (what was desirable for the analysis), images that contained cirrus clouds first needed to be selected. However, there were no labels provided for this task, so the criteria for determining whether an image contained cirrus clouds had to be experimentally decided. Visual observation of the cirrus bands made it clear that images with cirrus clouds had a much larger pixel value range than images without cirrus clouds. The minimum threshold for the range of pixel values was set to be 500.<sup>6</sup> Only 5,420 of the 26,671 original images satisfied this condition, with 2,152 “fire” images and 3,268 “non-fire” images.

#### 3.3.2 K-Means Clustering for Unsupervised Cirrus Image Segmentation

Image segmentation was conducted to simplify the features of the cirrus clouds. A  $128^2 \times 3$  ( $16,384 \times 3$ ) dimensional array, consisting of each pixel value of an image along with the pixel's coordinates on the image (ranging from 0 to 128), was fed into the K-Means Clustering algorithm with a K-value of 3.

**Clustering Hypothesis** It was hypothesized that if a K-value of 3 was used, the clustering algorithm would identify spatial regions in the image corresponding to degrees of cloud contamination: “dense” cirrus, “scattered” cirrus, and “no” cirrus.

The point of simplifying the features of the image from continuous pixel values to discrete three-class values was to allow a deep learning model to learn the associations between high-level cirrus cloud patterns and the presence of wildfires.<sup>7</sup> In rural regions of the Amazon Rainforest where computational power is a luxury, it is crucial to minimize computational expense while maximizing the accuracy of computer vision models, and image segmentation provided a proof of concept for this task.

#### 3.3.3 Cirrus-to-Wildfire CNN

To test the hypothesis that feature simplification could provide added benefits to wildfire detection algorithms, two convolutional neural networks were constructed: each with the same architecture but trained on different data features.

- **Benchmark Model (Only SWIR Data)** The benchmark model was trained only on the two Short-wave Infrared bands.
- **Experimental Model (SWIR and Cirrus Data)** The experimental model was trained on the segmented Cirrus bands stacked depthwise with the two Short-wave Infrared bands. An example of an input image can be seen in Section 4.2.1.

---

<sup>6</sup>In most images, raw pixel values hovered around 5,000.

<sup>7</sup>Section 5.2 also describes a relationship between cirrus pixels and fire pixels using these segmented cirrus images.

**Model Architecture** Both of the above models used the same architecture, hyperparameters, and random seed. The architecture had 1,824,937 trainable parameters, with most of the parameters concentrated in the final two convolution layers and the first fully connected layer. For this reason, L2 Regularization with a lamdba value of 3e-3 was used in the final two convolution layers, and dropout regularization with a dropout probability of 0.3 was used before flattening the outputs of the last convolution. The fully connected layers were also regularized with dropout, with dropout probabilities decreasing per layer from 0.3 to 0.1.

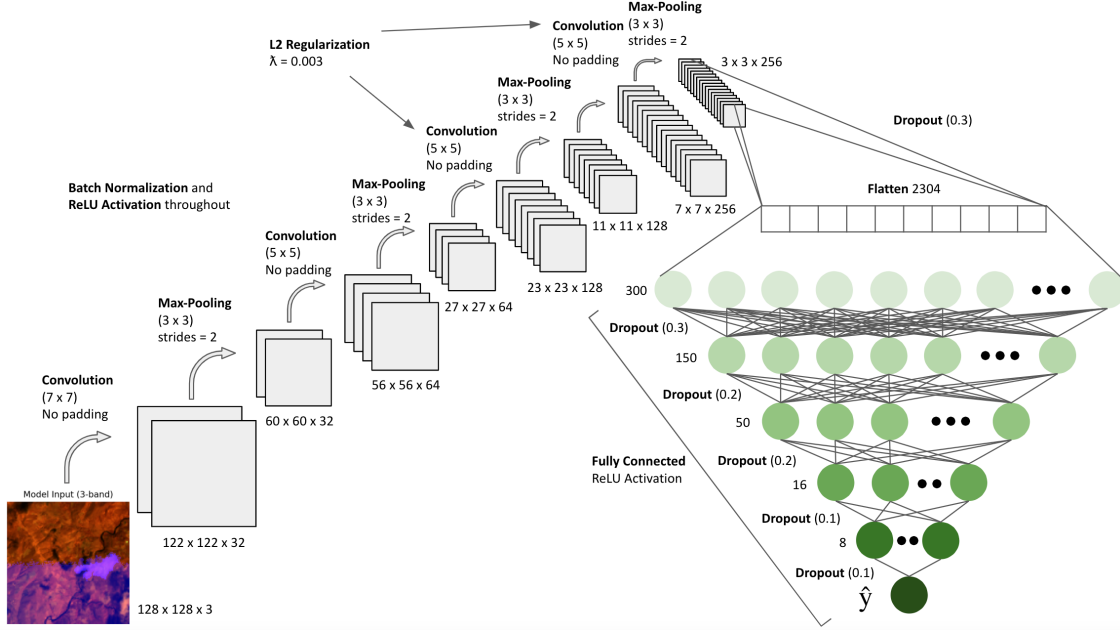


**Figure 5:** The convolutional model built for the binary classification task.

**Hypotheses** The null hypothesis was that the validation accuracy of the benchmark model would equal the validation accuracy of the experimental model. The alternative hypothesis was that the validation accuracy of the experimental model would exceed that of the benchmark model.

## 4 Results

### 4.1 Fully Convolutional Neural Network

#### 4.1.1 Learning Curves

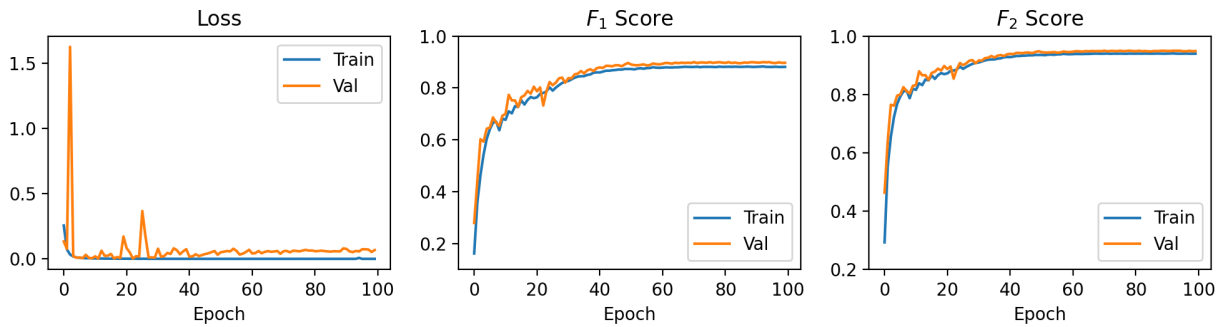


**Figure 6:** The train and validation performance of the FCN over 100 epochs.



The FCN quickly converged on the train set while the validation loss still experienced some noise until around epoch 50. After epoch 50, the validation loss seems to subtly increase, implying slight overfitting, but interestingly this is not reflected in the validation  $F_1$  and  $F_2$  Scores.

#### 4.1.2 Metrics and Confusion Matrix

	Actual Fire	Actual No Fire
Predicted Fire	TP = 18,691	FP = 2,607
Predicted No Fire	FN = 277	TN = 34,995,841

**Figure 7:** The confusion matrix of the FCN shows the proportion of real fires identified correctly (recall) and the proportion of predicted fires identified correctly (precision).

The FCN achieved a 0.962  $F_2$  score and a 0.928  $F_1$  score on the validation data set, corresponding to a Precision of 0.878 and a Recall of 0.989. This means that the model very rarely fails to identity an existing fire, but occasionally may be too sensitive and flag non-fire pixels as fire pixels. Visualizations of accurate predictions as well as predictions with false positives are shown below.

#### 4.1.3 Performance Visualizations

The following figure shows some examples of the models' predictions when there are a small number of pixels in the mask that contain an active fire. The left column depicts the input data, the middle column depicts the ground truth

mask, and the right column depicts the mask predicted by the FCN.

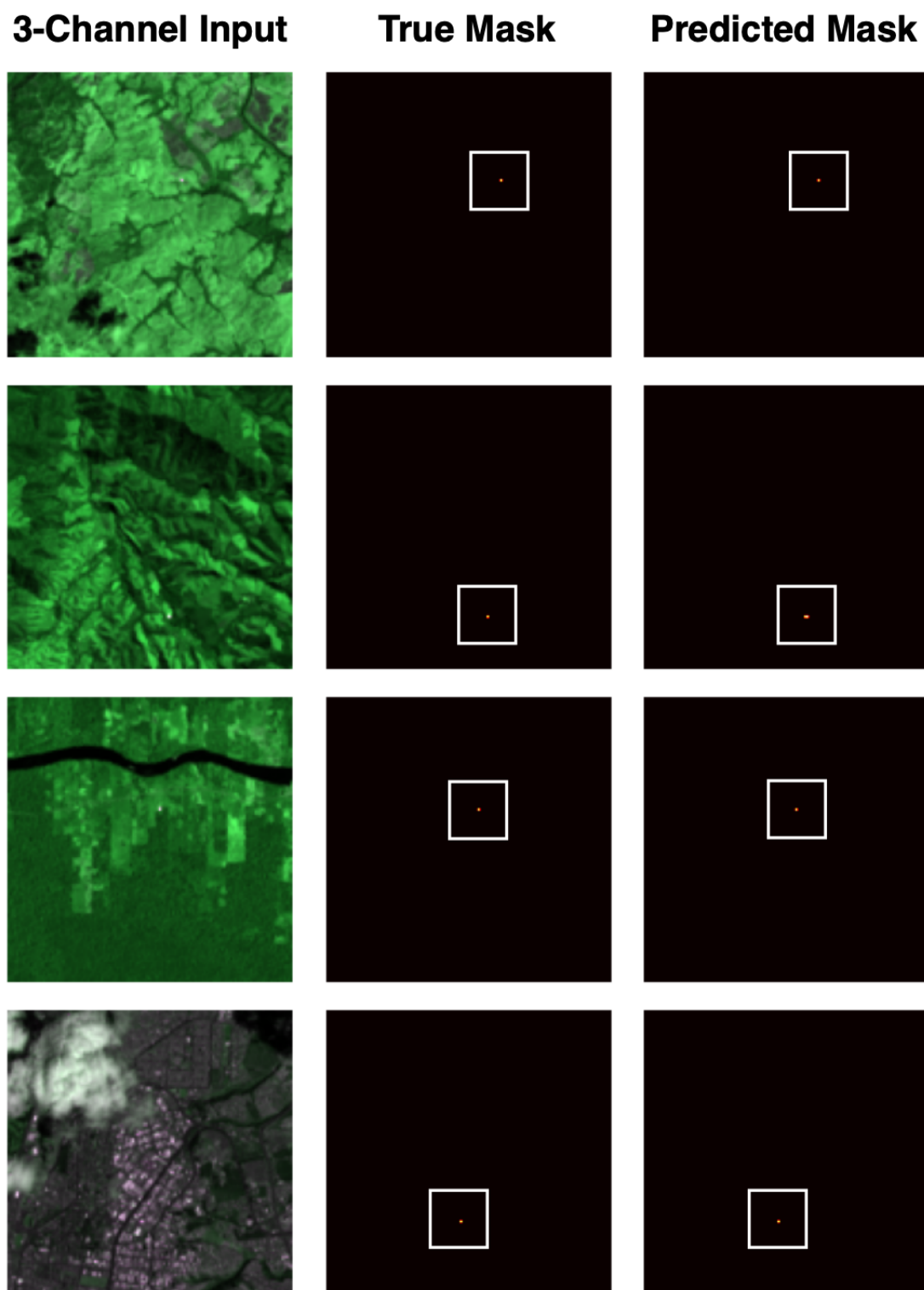


**Figure 8:** Mask predictions when the number of ground truth fires is small. The "fire" pixels are circled. represent pixels with active wildfires.

The following figure shows some examples of the models' predictions when there are a large number of pixels in the mask that contain an active fire. The third row shows that the model can fail to identify fire-absent pixels when they are surrounded by fire-containing pixels. This over-labeling of fires was, however, not observed when the mask had a very few number of fire pixels.

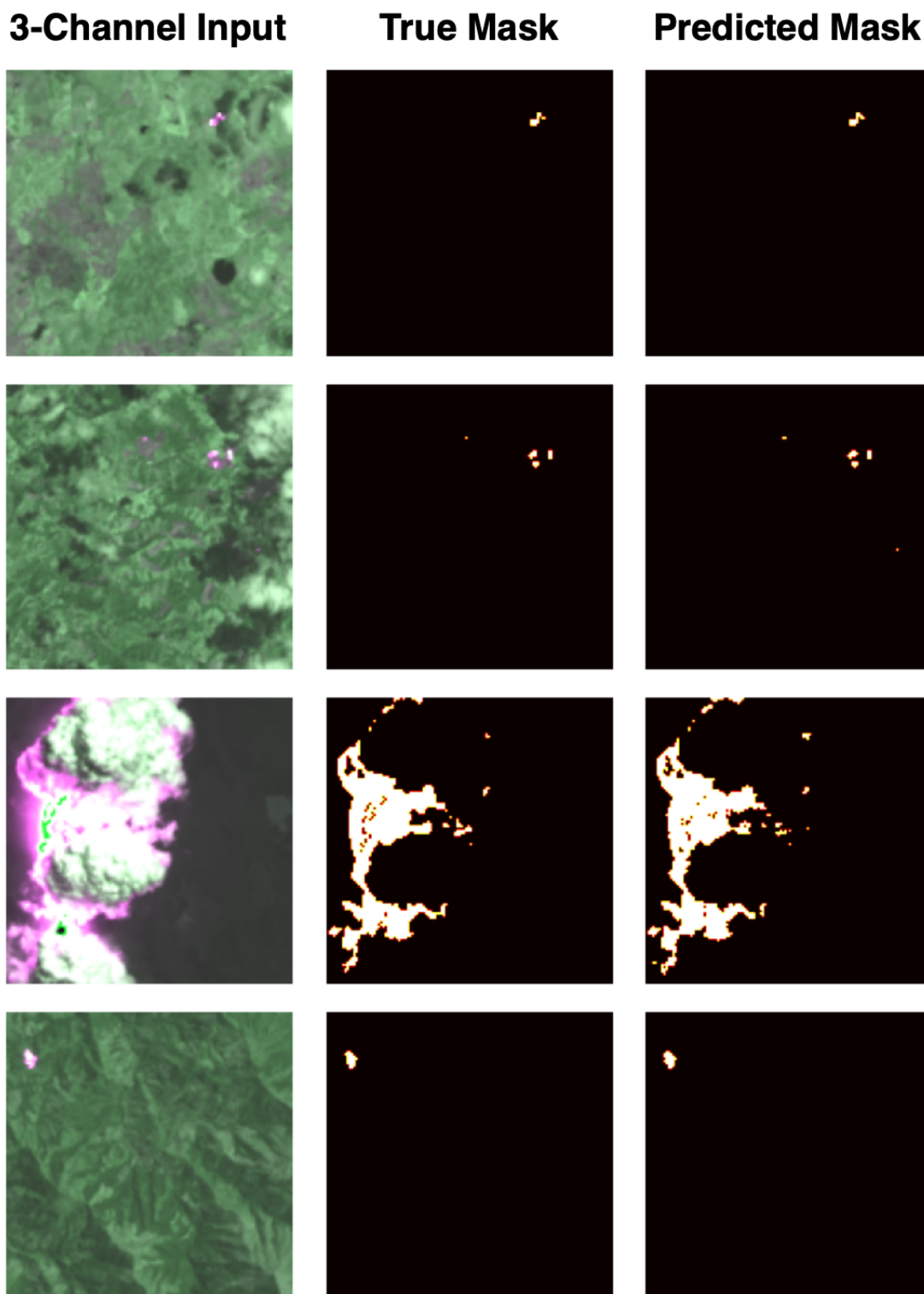


**Figure 9:** Mask predictions when the number of ground truth fires is large. False positives are more frequent.

#### 4.1.4 Model Testing Scenarios

**Geographical Test** The FCN was tested on 2,000 previously-unseen images from Guyana and Suriname. On this test data, the model achieved an  $F_1$  score of 0.875 and an  $F_2$  score of 0.934. These results confirm that the FCN can generalize well to data gathered from geographical regions that differ in topography and climate.

**Non-Fire Images Test** The FCN was also tested on 2,000 “non-fire” images. Of all the pixels in the 2,000 predicted masks, only 13 pixels were predicted to contain wildfires. In other words, the model was unable to completely eliminate false negatives, but kept the rate of false positives extremely low, at  $3.967\text{e-}5\%$ .

## 4.2 Cirrus Band Analysis

### 4.2.1 Unsupervised Image Segmentation

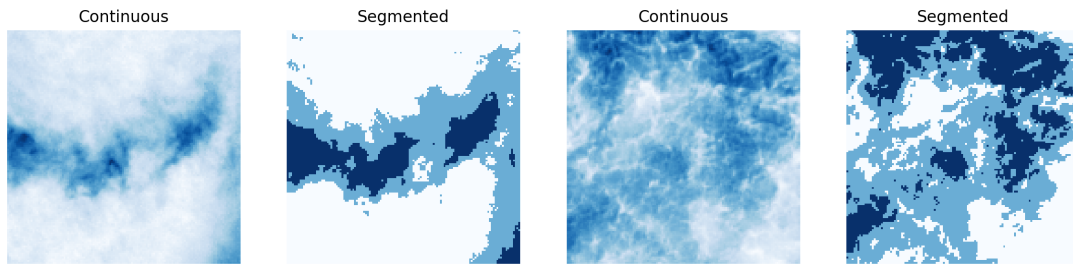


**Figure 10:** Cirrus band segmented by level of cirrus cloud contamination.

Visual observation supported the hypothesis that the K-Means clustering algorithm would find centroid values that account for the differing degrees of cirrus cloud contamination in the cirrus band.

### Model Inputs

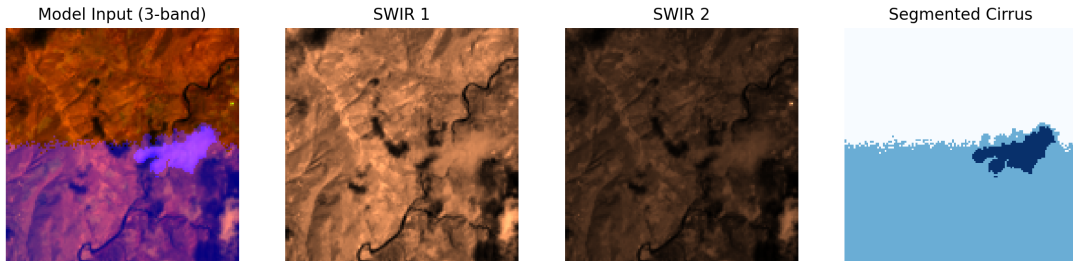


**Figure 11:** Inputs for the Experimental CNN. The Benchmark CNN did not have segmented cirrus images as inputs.

Though cirrus clouds are sometimes visible in the SWIR bands, adding the segmented cirrus band brought out the features of the clouds so that after min-max normalization was applied, the segmented cirrus channel would have more weight.

#### 4.2.2 Learning Curves and Metrics

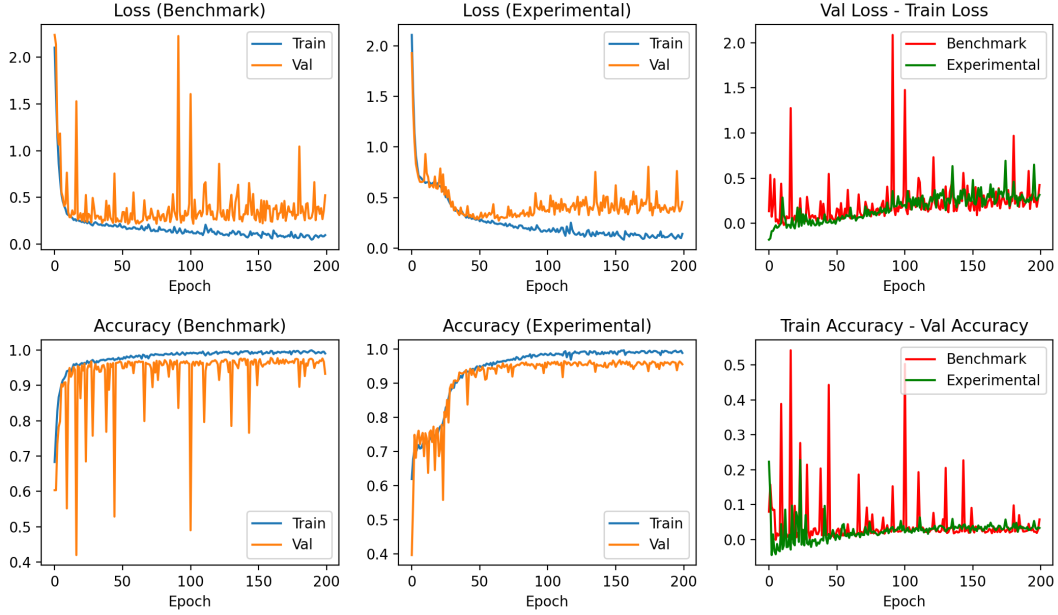


**Figure 12:** The train and validation performance of the Cirrus-to-Wildfire CNN over 250 epochs.

The benchmark model (introduced in Section 3.3.3) with the 2-channel SWIR inputs achieved a validation binary accuracy of 93.266%. The experimental model trained on 3-channel inputs consisting of the segmented cirrus band in addition to the two SWIR bands achieved a 95.572% validation binary accuracy.<sup>8</sup> The random seed and all hyperparameters described in Section 3.3.3 were held equal between the models.

The difference between the binary accuracies was 2.306%. The additional benefit of including the segmented cirrus bands can also be seen in the learning curves above. While the benchmark model had a high degree of noise, the experimental model had much smoother training. Though the validation accuracy of the benchmark model reached 90% around 25 epochs earlier than the validation accuracy of the experimental model, the latter maintained the plateau for around 165 more epochs while the former fluctuated unpredictably.

Since the experimental model proved to be more computationally stable while generalizing better on validation data, there was definitely a measurable increase in model performance when the segmented cirrus bands were included to forecast the presence of wildfires.

#### 4.2.3 Two Proportion Z-Test

A one-tailed two proportion z-test was conducted to assess the statistical significance of the observed difference in model performance between the benchmark and experimental models. Shown below are the calculations that confirmed a p-value of 0.00968. The p-value provides strong evidence that there including the segmented cirrus band

<sup>8</sup>The train set binary accuracy reached 99.8% for both models.

increases the accuracy of the Cirrus-to-Wildfire CNN. The null hypothesis was therefore rejected.

$$\begin{aligned}
H_0 : p_e - p_b &= 0 \\
H_A : p_e - p_b &> 0 \\
p_e &= 0.95572 \\
p_b &= 0.93266 \\
p_{pooled} &= \frac{p_e n_e + p_b n_b}{n_e + n_b} = \frac{p_e + p_b}{2} = 0.94419 \\
z &= \frac{p_e - p_b}{\sqrt{p_{pooled}(1 - p_{pooled})(\frac{2}{n})}} = 2.3387 \\
p &= \text{normalCdf}(z, \infty, 0, 1) = 0.00968
\end{aligned}$$

## 5 Discussion

### 5.1 Deep Learning Tasks

#### 5.1.1 FCN

The results of the FCN show that despite the class imbalance inherent to the data set, the model is still a highly effective discriminator between fire and non-fire pixels. In fact, of all pixels in the validation data set containing fires, the model had a false negative rate of 1.46%. This is an important trait when software is used for real-time wildfire detection in South America, since identifying all regions with ground truth fires (i.e. maximizing recall) is the first priority.<sup>9</sup>

A potential use case for the model involves is Land Cover Change Detection. Satellites or aerial vehicles can periodically conduct forward propagation, accessing the predicted probability that each pixel of land contains a wildfire at that instant. If the satellite or aerial vehicle takes snapshots of particular regions of land hourly, weekly, etc., then the fluctuations in the probabilities of each pixel could be analyzed using a time-series model to enhance the wildfire prediction task.

**Comparison of FCN with Other Models** The 34,525,121-parameter neural network designed by Pereira et al. (2021) was referred to by the authors as the “U-Net,” and their 2,161,649-parameter model was referred to as the “U-Net-Light” [11]. The performance of these models is compared with the performance of this research’s FCN in the table below.

Model	No. of Parameters	Precision	Recall	$F_1$	$F_2$
“U-Net”	34,525,121	0.898	0.888	0.893	0.890
“U-Net-Light”	2,161,649	0.908	0.861	0.884	0.870
<b>FCN</b>	<b>2,138,785</b>	<b>0.878</b>	<b>0.985</b>	<b>0.928</b>	<b>0.962</b>

The architecture of the FCN required and less regularization than the “U-Net” and “U-Net-Light,” which used dropout layers between convolutions. This corroborates the findings of Sun et al. (2021), who demonstrated that using a simpler architecture without regularization results in similar performance as using a more complex architecture with heavy regularization [15].

#### 5.1.2 Cirrus-to-Wildfire CNN

The success of the Experimental Cirrus-to-Wildfire CNN shows that feature simplification is a promising way to detect active wildfires. In other words, it has already been established (by other researchers and this paper) that not all ten Landsat bands have to be used to detect wildfires; the next step is to find even more optimal simplifications of the input data. For example, Principal Component Analysis (PCA) can compress the dimensionality of inputs, after which clustering the images can allow associations between bands and fire pixels to be found. In this manner, less data will be needed to train a more versatile model.

<sup>9</sup>As mentioned in Section 3.2.2, false negatives are more dangerous than false positives, which can be thought of as false alarms.

## 5.2 Relationship Between Cirrus Clouds and Wildfire Acreage

Recall that the pixel values of the cirrus bands were segmented into three cirrus contamination categories: dense, scattered, and none. These segmented images were analyzed in trying to find a correlation between the number of pixels in each category and the number of wildfire pixels in the corresponding mask. Each scatter plot below contains 5,420 data points, each data point representing one image in the data set for the Cirrus-to-Wildfire CNN.

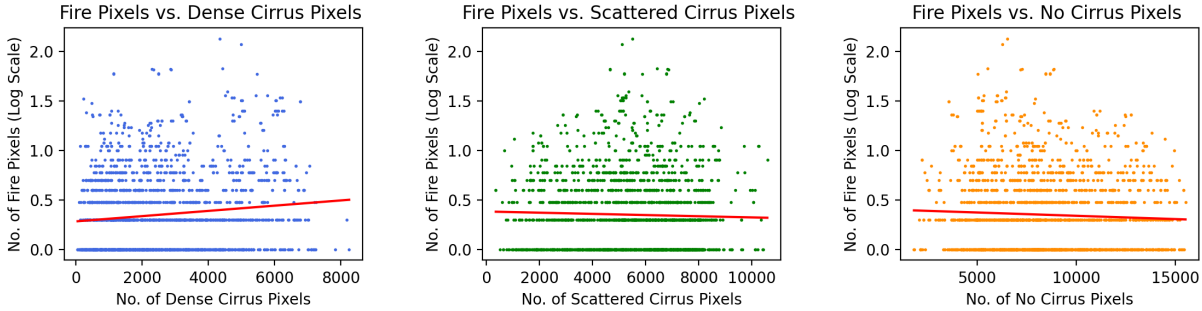


**Figure 13:** Scatter plots of the number of fire pixels against the number of pixels in each cirrus contamination class. Linear regression fits are included to give a sense of the data’s form and direction.

From the figures above, it appears that the plot of Fire Pixels vs. Dense Cirrus Pixels is similar to a y-axis reflection of the plot of Fire Pixels vs. No Cirrus Pixels. Furthermore, it appears that the plot of Fire Pixels vs. Scattered Cirrus Pixels is nearly symmetric. Notice that the curves formed by the boundary data points on the figures take on distinct shapes. The images with the largest number of fire pixels (points near the top of the graphs) appear on different regions from graph to graph: Specifically, these images have:

- More “Dense Cirrus” pixels than the mean number of “Dense Cirrus” pixels across all images.
- Similar numbers of “Scattered Cirrus” pixels as the mean number of “Scattered Cirrus” pixels across all images.
- Less “No Cirrus” pixels than the mean number of “No Cirrus” pixels across all images.

These findings reveal that there might be an underlying connection between a region’s degree of cirrus contamination and the probability of containing an active wildfire in that region, supporting Veselovskii et al. [17].

## 6 Conclusions

The computer vision models designed in this study are useful for Land Cover Change Detection, which involves monitoring wildfire hot spots periodically and conducting time-series analyses of pixel-wise probabilities to predict wildfires in advance. An  $F_2$  score of 0.962 and a high degree of generalizability prove the versatility of the fully convolutional model.

**Limitations** Limited computational power, which necessitated the reduction of the data set size, was one constraint faced throughout the course of this research. While other researchers have conducted active wildfire detection on data sets with more than one hundred thousand images, this data set only contained 14,274 images. However, excellent results on more than 6,000 validation and test images compensate for this data shortage.

**Need For Further Research** Further research should investigate whether the proposed relationship between the degree of cirrus cloud contamination correlates with the presence of an active wildfire. Perhaps, a larger meta-data set can be created from Landsat 8 imagery to analyze this relationship using more variables. Further research can also apply feature simplification to the coastal aerosol band in order to explore more optimal simplifications of the satellite imagery.

## Acknowledgement

I would like to thank Mr. Lordan for his time and feedback regarding the research in this paper.

## References

- [1] Aragão, L. E., Anderson, L. O., Fonseca, M. G., Rosan, T. M., Vedovato, L. B., Wagner, F. H., ... & Saatchi, S. (2018). 21st Century drought-related fires counteract the decline of Amazon deforestation carbon emissions. *Nature communications*, 9(1), 1-12.
- [2] Arana-Pulido, V., Cabrera-Almeida, F., Perez-Mato, J., Dorta-Naranjo, B. P., Hernandez-Rodriguez, S., & Jimenez-Yguacel, E. (2018). Challenges of an Autonomous Wildfire Geolocation System Based on Synthetic Vision Technology. *Sensors*, 18(11), 3631.
- [3] Dauphin, Y., & Cubuk, E. D. (2020, September). Deconstructing the Regularization of BatchNorm. In *International Conference on Learning Representations*.
- [4] Drozdal, M., Vorontsov, E., Chartrand, G., Kadoury, S., & Pal, C. (2016). The importance of skip connections applications in biomedical image segmentation. In *Deep learning and data labeling for medical applications* (pp. 179-187). Springer, Cham.
- [5] Khryashchev, V., & Larionov, R. (2020, March). Wildfire Segmentation on Satellite Images using Deep Learning. In *2020 Moscow Workshop on Electronic and Networking Technologies (MWENT)* (pp. 1-5). IEEE.
- [6] Kingma, D. P., & Ba, J. (2014). Adam: A method for stochastic optimization. *arXiv preprint arXiv:1412.6980*.
- [7] Knight, E. J., & Knight, G. (2014). Landsat-8 operational land imager design, characterization and performance. *Remote sensing*, 6(11), 10286-10305.
- [8] Matson, M., & Holben, B. (1987). Satellite detection of tropical burning in Brazil. *International Journal of Remote Sensing*, 8(3), 509-516.
- [9] Patro, S., & Sahu, K. K. (2015). Normalization: A preprocessing stage. *arXiv preprint arXiv:1503.06462*.
- [10] Pereira, G. H. D. A., Fusioka, A.M., Nassu, B. T., & Minneto, R. (2020). A Large-Scale Dataset for Active Fire Detection/Segmentation (Landsat-8). *IEEE Dataport*. [dx.doi.org/10.21227/t9gn-y009](https://dx.doi.org/10.21227/t9gn-y009)
- [11] Pereira, G. H. D. A., Fusioka, A. M., Nassu, B. T., & Minetto, R. (2021). Active Fire Detection in Landsat-8 Imagery: a Large-Scale Dataset and a Deep-Learning Study. *arXiv preprint arXiv:2101.03409*.
- [12] Ronneberger, O., Fischer, P., & Brox, T. (2015, October). U-net: Convolutional networks for biomedical image segmentation. In *International Conference on Medical image computing and computer-assisted intervention* (pp. 234-241). Springer, Cham.
- [13] Schroeder, W., Oliva, P., Giglio, L., Quayle, B., Lorenz, E., & Morelli, F. (2016). Active fire detection using Landsat-8/OLI data. *Remote sensing of environment*, 185, 210-220.
- [14] Sousa, M. J., Moutinho, A., & Almeida, M. (2020). Wildfire detection using transfer learning on augmented datasets. *Expert Systems with Applications*, 142, 112975.
- [15] Sun, C., Sharma, J., & Maiti, M. (2021). Investigating the Relationship Between Dropout Regularization and Model Complexity in Neural Networks. *arXiv preprint arXiv:2108.06628*.
- [16] Van Gansbeke, W., Vandenhende, S., Georgoulis, S., & Van Gool, L. (2021). Unsupervised semantic segmentation by contrasting object mask proposals. *arXiv preprint arXiv:2102.06191*.
- [17] Veselovskii, I., Hu, Q., Ansmann, A., Goloub, P., Podvin, T., & Korenskiy, M. (2021). Fluorescence lidar observations of wildfire smoke inside cirrus: A contribution to smoke-cirrus–interaction research. *Atmospheric Chemistry and Physics Discussions*, 1-29.